Influence of a Pore-Forming Agent on Swelling, Network Parameters, and Permeability of Poly(ethylene glycol)-Crosslinked Poly(methyl vinyl ether-*co*-maleic acid) Hydrogels: Application in Transdermal Delivery Systems

Thakur Raghu Raj Singh, Martin J. Garland, Katarzyna Migalska, Ester Caffarel Salvador, Rahamatullah Shaikh, Helen O. McCarthy, A. David Woolfson, Ryan F. Donnelly

School of Pharmacy, Queens University Belfast, Medical Biology Centre, 97 Lisburn Road, Belfast BT9 7BL, Northern Ireland, United Kingdom

Received 24 December 2010; accepted 17 November 2011
DOI 10.1002/app.36524
Published online 30 January 2012 in Wiley Online Library (wileyonlinelibrary.com).

ABSTRACT: We characterized hydrogels, prepared from aqueous blends of poly(methyl vinyl ether-*co*-maleic acid) (PMVE/MA) and poly(ethylene glycol) (PEG 10,000 Daltons) containing a pore-forming agent (sodium bicarbonate, $NaHCO_3$). Increase in $NaHCO_3$ content increased the equilibrium water content (EWC) and average molecular weight between crosslinks (M_c) of hydrogels. For example, the %EWC was 731, 860, 1109, and 7536% and the M_c was 8.26, 31.64, 30.04, and 3010.00×10^5 g/mol for hydrogels prepared from aqueous blends containing 0, 1, 2, and 5% w/w of $NaHCO_3$, respectively. Increase in $NaHCO_3$ content also resulted in increased permeation of insulin. After 24 h, percentage permeation was 0.94, 3.68, and 25.71% across hydrogel membranes prepared from aqueous blends containing 0, 2, and 5% w/w of $NaHCO_3$, respectively. Hydrogels containing the pore-forming agent were fabricated into microneedles (MNs) for transdermal drug delivery applications by integrating the MNs with insulin-loaded patches. It was observed that the mean amount of insulin permeating across neonatal porcine skin *in vitro* was 20.62% and 52.48% from hydrogel MNs prepared from aqueous blends containing 0 and 5% w/w of $NaHCO_3$. We believe that these pore-forming hydrogels are likely to prove extremely useful for applications in transdermal drug delivery of biomolecules. © 2012 Wiley Periodicals, Inc. J Appl Polym Sci 125: 2680–2694, 2012

Key words: hydrogels; poly(methyl vinyl ether-*co*-maleic anhydride); poly(methyl vinyl ether-*co*-maleic acid); poly(ethylene glycol); pore-forming agent; insulin

INTRODUCTION

Hydrogels are crosslinked polymeric structures composed of hydrophilic homo- or hetero-*co*-polymers, arranged in a three-dimensional structure. Hydrogels can absorb and retain significant amounts of water without being dissolved, which makes them ideal for controlled drug delivery applications.[1–5]

Current applications of hydrogels, such as in wound dressings, absorbents, scaffolds for tissue culturing and biosensors, are dependent upon their swelling and diffusional properties. These, in turn, are controlled mainly by crosslinking density.[4,6–9] Swelling behavior of hydrogels can be dramatically affected by changes in external pH, temperature, ionic strength, type of crosslinking agent, and electromagnetic radiation.[10] The crosslinks in hydrogels provide the characteristic network structures, or the pore-size, which, in turn, controls the swelling of hydrogel materials in a given solvent.[11,12] Furthermore, the amount of crosslinking agent used in the hydrogel is directly related to the crosslink density that, accordingly, controls the diffusion coefficient of the solute. In addition, the hydrodynamic radius, molecular weight, and physicochemical properties of the solute control its diffusion. Hydrogels with higher crosslink density show lower diffusion coefficients for solutes and vice versa.[13] Diffusion of solutes in hydrogels has applications in a wide variety of fields, such as in separation processes like chromatography, in biosensors, and in biomaterials for delivery of bioactive agents.[14–16] However, applications of hydrogels may be limited if the pore-size is smaller than the solute size, especially in delivery of high molecular weight solutes (e.g., peptides and proteins). In such a scenario, hydrogels with larger pores would be highly desirable.[17] Therefore, to

Correspondence to: R. F. Donnelly (r.donnelly@qub.ac.uk).
Contract grant sponsor: Biotechnology and Biological Sciences Research Council; contract grant number: BB/E020534/1.
Contract grant sponsor: Wellcome Trust; contract grant number: WT094085MA.

optimize hydrogel systems for a particular application, it is important to understand the principal parameters in solute diffusion within hydrogels, as well as the means by which they affect diffusion.[18]

Hydrogels can be divided into three different types in terms of solute diffusion, namely, macroporous hydrogels, microporous hydrogels, and nonporous hydrogels. The pore-sizes of macroporous hydrogels range from 200 to 1000 Å and those of microporous hydrogels range from 50 to 200 Å.[16] For controlled-release systems, pore-size and distribution of pores affect release kinetics of solutes. Several techniques have been used in fabrication of porous polymeric materials, such as, freeze-drying,[19–22] gas foaming/salt leaching,[23] phase separation,[24] fiber bonding,[25] porosigen,[26,27] and 3D printing.[28] An appropriate technique should be used in fabrication of porous structures. Hydrogels prepared by the gas blowing technique are also called "hydrogel foams" due to the foaming process used in their preparation.[29,30] Chen[31] reported that the gas blowing technique was capable of producing porous hydrogels with pore radii in the order of few hundreds of microns.

The average pore-size, the pore-size distribution, and the pore interconnections (together termed "tortuosity") are important factors in controlling solute diffusion in hydrogels. In addition to solute size, the type and strength of interactions of solute with the polymer chains of the hydrogel are also important in governing solute diffusion.[6] Understanding network structure and transport behavior of solutes through hydrogels is essential in modeling solute release from candidate hydrogels-based controlled drug delivery systems. Hydrogel-based controlled release drug delivery systems are intended to provide the drug of interest in a predetermined concentration to fulfil specific therapeutic needs.[1]

We have previously demonstrated[32] the swelling kinetics and network parameters of poly(ethylene glycol) (PEG)-crosslinked poly(methylvinylether/maleic acid) (PMVE/MA) hydrogels. It was observed that hydrogels crosslinked with PEG with a molecular weight of 10,000 Da showed the highest degree of swelling at equilibrium, followed by those crosslinked by PEG 1000 and then those crosslinked with PEG 200. This higher degree of swelling in hydrogels crosslinked with PEG 10,000 Da was due to the lower crosslink density of the hydrogel. Consequently, we have shown efficient diffusion of theophylline, vitamin B_{12}, and fluorescein sodium across such hydrogels.[33] In general, the permeability and diffusion coefficients of all three solutes decreased with increase in PMVE/MA content. In addition, permeability and diffusion coefficient values increased with decrease in the hydrodynamic radii of the solute molecules.[33] However, macromolecules, such as insulin with a hydrodynamic radius of 27 Å,[34] did not efficiently permeate across such hydrogels. This was due to the relatively small pore-sizes of PEG (10,000 Da) crosslinked PMVE/MA hydrogels and the higher hydrodynamic radius of insulin.

Peptide molecules, despite their relatively large hydrodynamic radii can be released from hydrogels with high porosity. Therefore, to produce porous hydrogels, in this study, we have investigated the effect of a pore-forming agent, sodium bicarbonate ($NaHCO_3$), on the swelling kinetics, network parameters, and permeation of a model peptide, insulin, from PEG-crosslinked PMVE/MA hydrogels. Transdermal delivery of biomolecules avoids gastrointestinal breakdown and first-pass hepatic metabolism. However, the skin's *stratum corneum* barrier prevents efficient absorption of these macromolecules. Accordingly, we then sought to formulate microneedle arrays (MN) from the hydrogels to bypass the *stratum corneum* and achieve controlled transdermal delivery of insulin. MN (50–900 μm in height, up to 2000 MN cm^{-2}) are minimally invasive devices that can be used to by-pass the *stratum corneum* barrier and thus achieve enhanced transdermal drug delivery.

EXPERIMENTAL

Materials

Gantrez® AN-139, a copolymer of methyl vinyl ether and maleic anhydride (PMVE/MAH, $M_w = 1{,}080{,}000$ daltons) was a gift from ISP Corp. Ltd., Guildford, UK. Poly(ethylene glycols) (PEGs) of MW 10,000 daltons were obtained from Sigma-Aldrich (Steinheim, Germany, UK). Poly(ester) film, one-side siliconized, release liner (FL2000™ PET 75 μ 1S) was obtained from Rexam Release BV (Apeldoorn, The Netherlands). Glisseal®N vacuum grease was purchased from Borer Chemie (Zuchwil, Switzerland). Resealable poly(ethylene) bags (101 × 140 mm^2) were obtained from Agar Scientific (Essex, UK).

Preparation of hydrogels

Aqueous polymeric blends were prepared using the required weight of PMVE/MAH, which was added to water (reagent grade 1) and stirred vigorously to ensure complete wetting and prevention of aggregation. The mixture was then heated and maintained between 95 to 100°C until a clear solution was obtained, this process causes hydrolysis of the anhydride moieties of PMVE/MAH to the free acid forms, yielding PMVE/MA.[35] Upon cooling, the required amount of 7.5% w/w aqueous solution of PEG was added to the aqueous blends of 15% w/w of PMVE/MA, containing 0, 1, 2, or 5% w/w of

$NaHCO_3$ and the casting blend was adjusted to final weight with water.

Films were prepared by slowly pouring the aqueous blend (30 g) into a mould consisting of a release liner (with siliconized side up) secured to a Perspex® base plate using a stainless steel clamp. Once assembled, the internal dimensions available for casting were 100 × 100 mm^2. The mould was placed on a leveled surface to allow the blend to spread evenly across the area of the mould. The cast blend was dried for 48 h at room temperature. After drying, the films were cured at 80°C for 24 h to induce chemical crosslinking between PMVE/MA and PEG.[32,33,35]

Dynamic and equilibrium swelling studies

Crosslinked film sheets (1.0 × 1.0 cm^2) of the above formulations were weighed in the dry state (m_o, xerogels) and were swollen in phosphate-buffered saline (PBS) at pH 7.4 ± 0.05 for 24 h at room temperature. At regular intervals, the sheets were removed, blotted with filter paper to eliminate excess surface water, and weighed (m_t, hydrogels). Hydrogel sheet samples at equilibrium were weighed (m_e) and were dried under vacuum at 80°C for 24 h to obtain extracted xerogels, which were weighed again (m_d). The percentage swelling, %S, and equilibrium water content, EWC, were calculated by using eqs. (1) and (2), respectively.[36]

$$\% \text{ Swelling} = \left(\frac{m_t - m_o}{m_o}\right) \times 100\% \quad (1)$$

$$\text{EWC} = \frac{m_e - m_d}{m_d} \times 100\% \quad (2)$$

To examine the controlling mechanism of the swelling process of PEG-crosslinked PMVE/MA hydrogels, the following second order kinetic model [eq. (3)] was used to process the experimental data[37]:

$$t/S = A + Bt \quad (3)$$

where, A is the reciprocal of the initial swelling rate of the hydrogel, r_o, or $1/(k_s S_{eq}^2)$, where k_s is the swelling rate constant, and B is the inverse of the degree of swelling at equilibrium, S_{eq}. To analyse the kinetic model, t/S versus t graphs were plotted and respective swelling rate parameters were determined.

Analysis of mechanism of water uptake, diffusion coefficient, and network parameters of hydrogels

Dynamic swelling studies were undertaken to elucidate the mechanism of water diffusion into the polymer samples, as determined by the dynamic portion of the gravimetric curve. Equation (4) was used to process the kinetic data of the swelling process to gain insights into the mechanism of water transport through the hydrogels.[4] The portion of the water absorption curve with a fractional water uptake (M_t/M_∞) less than 0.60 was analyzed with eq. (4).

$$\frac{M_t}{M_\infty} = k\, t^n \quad (4)$$

where, M_t is the mass of water absorbed at time t, M_∞ is the water uptake at equilibrium and k is a gel characteristic constant, and n is the swelling exponent. The k value is depended on the structural characteristics of the polymer and its interaction with the solvent and n describing the mechanism of penetrant transport into the hydrogel. The k and n is calculated from the intercepts and slopes of the plots of $\ln(M_t/M_\infty)$ versus $\ln t$. Fickian diffusion and Case II transport are defined by n values of 0.5 and 1, respectively. Anomalous transport behavior (non-Fickian diffusion) is intermediate between Fickian and Case II (relaxation controlled). This is reflected by n being between 0.5 and 1.[38,39]

For calculation of the diffusion constant of solvent into the hydrogels, eq. (5) was employed[4]:

$$\frac{M_t}{M_\infty} = F = 4\left(\frac{Dt}{\pi l^2}\right)^{1/2} \quad (5)$$

where, F is the fractional water uptake (M_t/M_∞) at time t and l is the thickness of the dry sample measured using a digital micrometer (Hilka, Pro-Craft, England, UK) and D is the diffusion coefficient.

Hydrogel network structure characterization is a complex procedure because of the many types of possible networks, which including, regular, irregular, loosely/highly cross-linked, and imperfect networks. As a result of these variations in the network structure, only average values of molecular weight between crosslinks are typically represented. For this, a range of experimental and theoretical methods can be employed.[16] In this study, the number average molecular weight between cross-links, M_c, was determined. M_c affects the mechanical, physical, and thermal properties of crosslinked polymeric systems. M_c can be determined by swelling studies according to the Flory and Rehner equation, eq. (6).[38,39] The volume fraction of a polymer, ϕ, in the swollen state describes the amount of liquid that can be imbibed into a hydrogel and is described as a ratio of the polymer volume to the swollen gel volume [eq. (7)].

$$M_C = \frac{-d_\rho V_s \phi^{1/3}}{[In(1-\phi) + \phi + \chi\phi^2]} \quad (6)$$

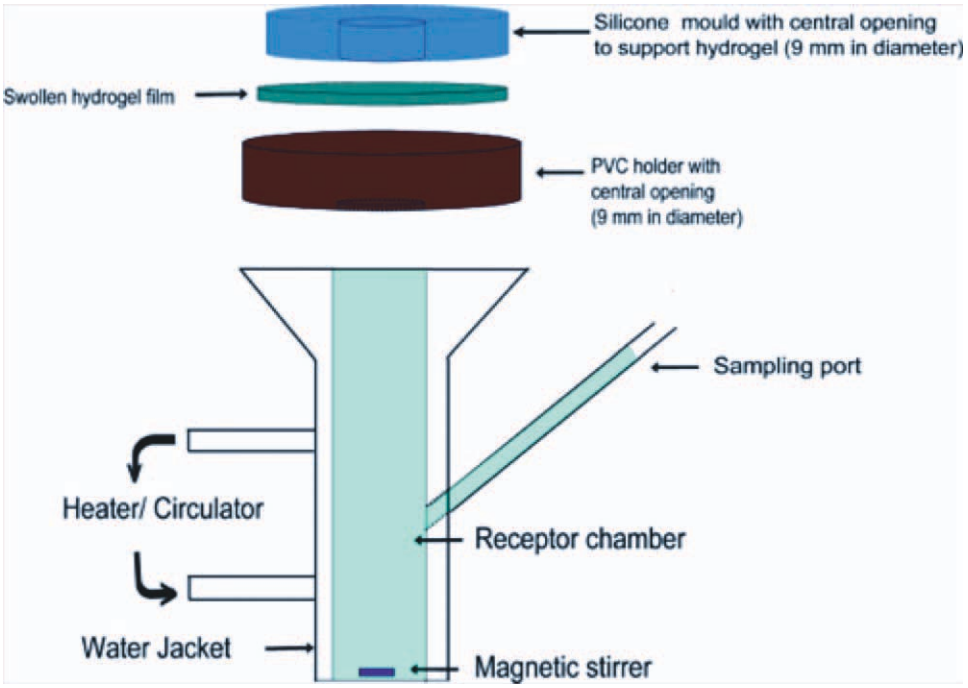

Figure 1 Illustration of the modified Franz-cell apparatus used to study permeation of insulin across swollen hydrogel membranes. [Color figure can be viewed in the online issue, which is available at wileyonlinelibrary.com.]

V_s is the molar volume of water (18 cm^3/mol), χ is the Flory-Huggins polymer-solvent interaction parameter.

$$\phi = \left[1 + \frac{d_\rho}{d_s}\left(\frac{m_a}{m_b}\right) - \frac{d_\rho}{d_s}\right]^{-1} \quad (7)$$

m_a and m_b are the mass of polymer before and after swelling and d_ρ and d_s are the densities of polymer and solvent, respectively. The density of the polymeric films was calculated using the following formula; $d_\rho = w/SX$, where X is the average thickness of the film, S is the cross-sectional area, and w the dry weight of the film.[40]

The polymer–water interaction parameter (χ) reflects the thermodynamic interaction in hydrogels which, in turn, indicates the change of interaction energy when polymer and solvent mix together. The χ parameters of hydrogels can be obtained experimentally via eq. (8)[41]:

$$\chi = \frac{1}{2} + \frac{\phi}{3} \quad (8)$$

Equation (8) neglects the M_c dependence of the χ parameter and, therefore, eq. (8) indicates that the χ values are always ≥ 0.50.

Permeation of hydrogels

Permeation studies for insulin were performed using the modified Franz-cell apparatus (PermeGear Inc, Bethlehem, PA) shown in Figure 1. The orifice diameter in both donor and receptor compartments was 9.0 mm. Receptor compartment volumes, $\sim$ 5.0 mL, were exactly determined by triplicate measurements of the weights of water they could accommodate. Account was taken of the volumes occupied by Teflon®-coated magnetic stirring bars. A poly(vinyl chloride) (PVC) holder, with orifice diameter of 9.0 mm, was placed on top of the receptor compartment. The swollen hydrogel membrane was then placed carefully in the PVC holder, making sure that no air-bubbles were formed underneath. A silicone mould, with orifice diameter of 9.0 mm, was placed onto the swollen hydrogel film, to avoid hydrogel movement during the period of study. Finally, a 100 μL aliquot of insulin solution (2.0 mg/mL) was placed on top of the hydrogel film and then the assembly was clamped using stainless-steel clamps and covered with laboratory film (Parafilm®, Pechiney plastic, WI). A water jacket surrounded the cells and was maintained at 37°C. Solutions were agitated at a speed of 600 rpm using small magnetic stirrers. The receptor phase was 0.1*M* Tris pH 10 (to maintain insulin stability and solubility and preserve sink conditions) and was degassed prior to use by sonication. Samples of 200 μL were removed at predetermined intervals and replaced with equal amounts of fresh degassed and prewarmed 0.1*M* Tris pH 10. The concentrations of insulin in the receiver medium were determined by HPLC analysis, as described below.

Pharmaceutical analysis of insulin

Insulin analysis was performed using RP-HPLC (Agilent 1200® Binary Pump, Agilent 1200®, Standard Autosampler, Agilent 1200® Variable Wavelength Detector, Agilent Technologies UK Ltd, Stockport, UK) with UV detection at 214 nm, as described previously.[42] Briefly, gradient separation was achieved using a RP C_4 (4.6 × 50.0 mm^2, 5.0 μm packing) Symmetry® 300 (Waters associates, UK) analytical column. The mobile phase gradient consisted of acetonitrile (ACN) and 0.1% v/v trifluoroacetic acid (TFA) aqueous solution. The gradient linearly changed from 25 : 75 (ACN : TFA) to 35 : 65 in 5 min followed by a 3 min isocratic 35 : 65 ratio and a 7 min re-equilibration period. The injection volume was 20 μL and elution was at a flow rate of 0.6 mL/min. The chromatographs obtained were analysed using Agilent ChemStation® Software B.02.01. The limit of detection was 0.77 μg/mL and the limit of quantification was 2.33 μg/mL.

Scanning electron microscopy

Scanning electron microscopy (SEM) of selected hydrogel samples was performed to investigate their morphology. Hydrogel samples were first swollen to equilibrium in PBS at room temperature, quickly frozen in liquid nitrogen thereafter and further freeze-dried in a VirTis freeze drier (Advantage XL-70, SP industries, NY, USA) under vacuum at −42°C for at least 48 h until all the solvent was sublimed. Freeze-dried hydrogels were then carefully fractured and their interior morphology were studied using SEM (JEOL 100 CXII, Transmission Electron Microscope, Tokyo, Japan). Before SEM observation, specimens of the hydrogel were fixed onto aluminium stubs and coated at 2.5 Kv, 18 mA with gold for 45 sec (POLARON E5150, Gold Sputter Coater, Quorum Technologies, East Sussex, UK).

Fabrication of microneedle arrays

MN arrays were prepared from each of the aqueous blends described above using laser-engineered silicone micromould templates, as described previously.[42,43] Briefly, silicone elastomer was poured into a custom-made aluminium mould and cured overnight at 40°C. A laser-machine tool (BluLase® Micromachining System, Blueacre Technology, Dundalk, Ireland) with a laser (Coherent Avia, Coherent Inc., Pittsburgh) emitting a beam having a wavelength of 355 nm and a pulse length of 30.0 ns (variable from 1 to 100 kHz) was then employed to produce MN moulds (11 × 11 array, 600 μm height, 300 μm width, and 300 μm interspacing at MN base). Aqueous blends (0.5 g) were then poured into the silicone micromoulds, centrifuged for 15.0 min at 3500 rpm and allowed to dry under ambient conditions for 48 h. After drying, the MN were cured at 80°C for 24 h, as described above for the corresponding films formulations, before removal from the moulds.

Measurement of MN break strength

The effect of hydrogel composition on mechanical strength (MN break strength) of formed and cured MN was assessed as described previously.[42,43] In brief, an axial compression load was applied to the MN arrays using a TA.XT-plus Texture Analyser (Stable Micro Systems, Surrey, UK). MN arrays were attached to the moving testing probe of the Texture Analyser using double-sided adhesive tape. The test station pressed MN arrays against a flat block of aluminium with a force of 0.36 N/needle for 30 s, at a rate of 0.5 mm/s. Pretest and posttest speeds were 1.0 mm/s and the trigger force was 0.049 N. Before and after fracture testing, all MN of each array were visualized using a light microscope (GXMGE-5 USB Digital Microscope, Laboratory Analysis Ltd, Devon, UK). The height of the MNs before and after testing was measured using the ruler function of the microscope software so that the percentage change in the MN height could be calculated.

Measurement of force required for MN insertion

The force required to insert PEG-crosslinked PMVE/MA MN array into excised neonatal porcine skin was determined using a TA.XT-plus Texture Analyser (Stable Micro Systems, Surrey, UK), as described previously.[43] Neonatal porcine skin was obtained from stillborn piglets and immediately (<24 h after birth) excised and trimmed to a thickness of 700 μm using an electric dermatome (Integra Life Sciences ™, Padgett Instruments, NJ). Skin was then carefully shaved (Mach 3 Power®, Gillette UK Ltd, Reading, UK) and stored in aluminium foil at −20°C until further use. Skin barrier function was confirmed as intact on a case by case basis by standard transepidermal water loss measurements (Delfin Vapometer®, Delfin Technologies Ltd, Paris, France). Any skin samples showing impaired barrier function were discarded.

Using double-sided adhesive tape, MN arrays were carefully attached to the moveable cylindrical probe. The *stratum corneum* surface of the skin was dried with tissue paper and the skin was placed, dermis side down, on a 500 μm thick sheet of dental wax. This assembly was then secured on a wooden block for support. The probe was lowered onto the skin at a speed of 0.5 mm/s until the desired force was exerted. Forces were held for 30.0 s and were increased gradually to the force at which MN penetration into skin was observed. After removal of MN arrays, a methylene blue solution (1.0 mg/mL) was

applied to the upper surface of the epidermis for 20 min so MN created pores within the skin could be visualized. Excess solution was gently wiped from the skin surface with dry tissue paper and then with normal saline solution. Subsequently, skin was imaged using a digital camera (Nikon Coolpix® s3100, Nikon UK Ltd, Surrey, UK).

Optical coherence tomographic assessment of MN penetration into neonatal porcine skin

The penetration characteristics of MN arrays (containing either 0% or 5% $NaHCO_3$) following insertion into excised neonatal porcine skin (thickness 1.0 mm), obtained and handled as above, was determined using Optical coherence tomography (OCT). MN were inserted into skin using the spring-activated applicator,[44] at a force of 11.0 N per array, and immediately viewed using an EX1301 OCT Microscope (Michelson Diagnostics Ltd, Kent, UK). Furthermore, following insertion into skin, a circular steel weight (diameter 11.0 mm, 3.5 g mass) was placed on top of the MN array, and the skin sample stored within an agar petri dish for a period of 24 h. After 24 h, the MN array was viewed using the EX1301 OCT Microscope to enable a measurement of the changes of the MN dimensions following residence within the skin.

The swept-source Fourier domain OCT system has a laser centre wavelength of 1305.0 ± 15.0 nm, facilitating real time high resolution imaging of the upper skin layers (7.5 μm lateral and 10.0 μm vertical resolution). The skin was scanned at a frame rate of up to 15 B-scans (2D cross-sectional scans) per second (scan width = 2.0 mm). 2D images were analysed using the imaging software ImageJ®. The scale of the image files obtained was 1.0 pixel = 4.2 μm, thus allowing accurate measurements of the depth of MN penetration, the width of pore created, and the distance between the MN base plate and the *stratum corneum*. To allow differentiation between MN and skin layers false colors were applied using Ability Photopaint® Version 4.14. In all instances, five replicates were performed, and >25 MN measured for each replicate.

Preparation of insulin-loaded adhesive transdermal patches

Adhesive patches containing insulin were prepared using a casting method, from aqueous blends containing 10% w/w PMVE/MA and 5% w/w tripropyleneglycol methyl ether (TPM). The required amount of insulin to produce patches with loadings of 5.0 mg/cm^2 was dissolved in the appropriate amount of 0.01*M* HCl necessary to dilute 30% w/w PMVE/MA stock solution to 10% w/w PMVE/MA. Next, the required amount of TPM was added. An aliquot (2.7 g) of the gel containing insulin was cast into the mould of 30 × 30 mm^2 dimensions and was left to dry for 48 h in order to form adhesive patches. The insulin content in prepared patches was analysed by HPLC, as described above, following patch dissolution. To examine the secondary structure of insulin after encapsulation and release from adhesive patches, circular dichroism (CD) was employed. CD spectra were obtained with a Jasco J-185 spectropolarimeter equipped with a temperature controller. CD spectra were collected at 20.0°C using a 1 cm quartz cell over the wavelength range of 200–400 nm. A resolution of 0.1 nm and scanning speed of 200 nm/min were employed. Samples for CD analysis were prepared by dissolution in 0.01*M* HCl. The spectra of insulin samples with concentrations of approximately 0.025 mg/mL were compared with that of fresh insulin in 0.01*M* HCl.

Insulin-loaded delivery systems were produced by attaching adhesive patches to the upper surfaces of formed and cured MN arrays using gentle pressure.

In vitro insulin permeation studies

Diffusion of insulin from integrated MN-adhesive patch delivery systems across neonatal porcine skin was investigated *in vitro* using modified Franz diffusion cells (FDC-400 flat flange, 15 mm orifice diameter, mounted on an FDCD diffusion drive console providing synchronous stirring at 600 rpm and thermostated at 37.0°C ± 1.0°C) (Crown Glass Co. Inc., Sommerville, NJ). Receptor compartment volumes, ~ 12.0 mL, were exactly determined by triplicate measurements of the weights of water they could accommodate. Neonatal porcine skin was obtained from stillborn piglets and immediately (<24 h after birth) excised, trimmed to a thickness of 300 ± 50 μm using the dermatome, and frozen in liquid nitrogen vapour. Skin was then stored at −20.0°C until further use. Shaved (as described above) skin samples were pre-equilibrated in receptor medium (again 0.1*M* Tris buffer pH 10) for 1.0 h before beginning the experiments. A circular specimen of the skin was secured to the donor compartment of the diffusion cell using cynoacrylate adhesive (Loctite, Dublin, Ireland) with the *stratum corneum* side facing the donor compartment. Using a custom spring-loaded applicator[43] integrated MN-adhesive patch delivery systems were inserted with an application force of 11.0 N/array into the centre of the skin. MNs were kept in place during the experiment by the application of a non-adhesive putty material (BluTac®, Bostik Ltd., Leicester, UK) to their upper surface. With MN arrays in place, donor compartments were mounted onto the receptor compartments of the Franz cells. Using a long needle, samples

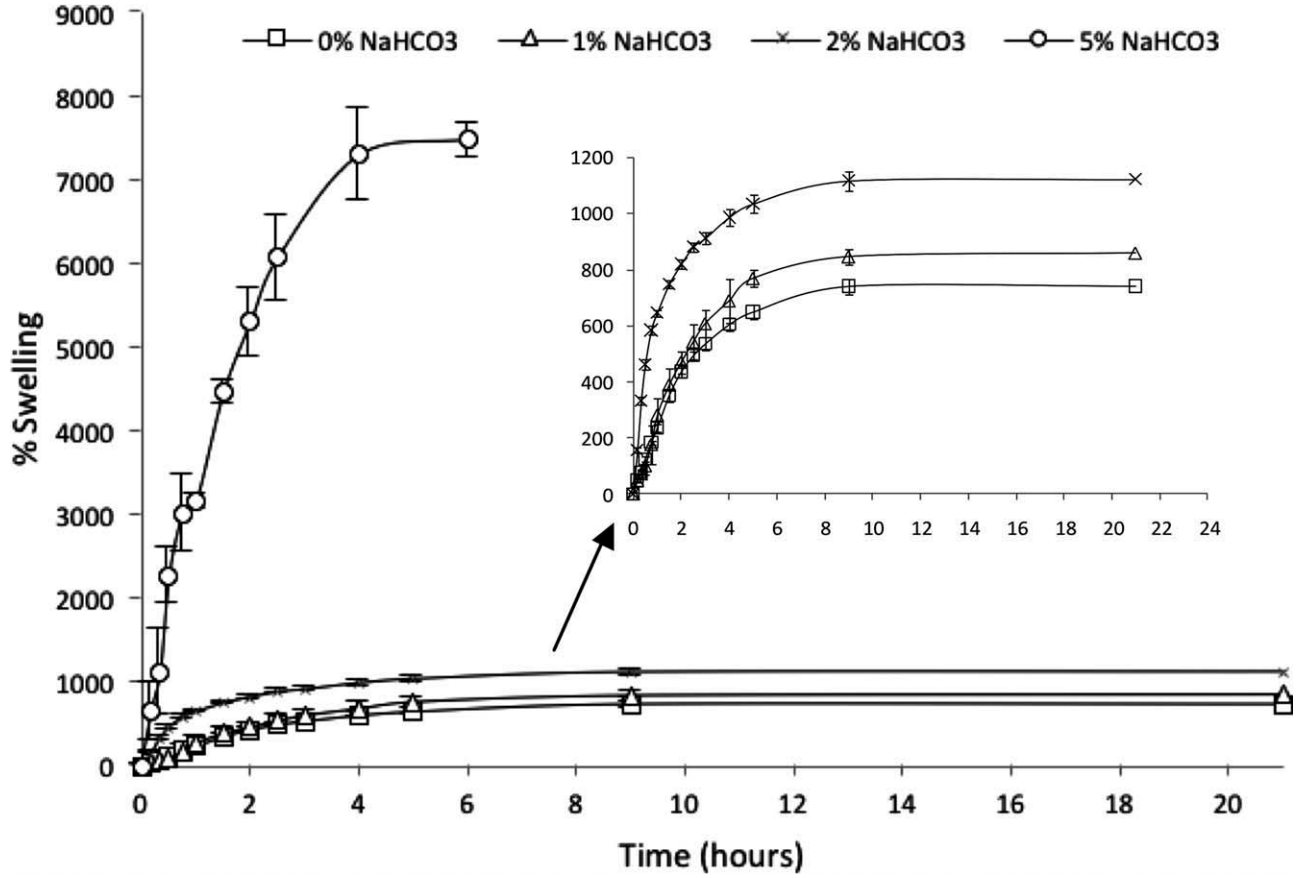

Figure 2 Percentage swelling of PEG-crosslinked PMVE/MA hydrogels containing different concentrations of $NaHCO_3$. Inset shows magnified view of swelling of hydrogels containing 0, 1, and 2% of $NaHCO_3$. Mean ± SD, $N = 3$.

(0.30 mL) were removed from the receptor compartment at defined time intervals and replaced with an equal volume of 0.1*M* Tris buffer pH 10. Sink conditions were maintained throughout the experiment. The concentrations of insulin in the receiver medium were determined by HPLC analysis, as described above.

Statistical analysis of data

One-way analysis of variance was used to assess the significance of the differences among different groups. Tukey's-HSD *posthoc* test was used to compare the means of different treatment groups. Results with $P < 0.05$ were considered to be statistically significant.

TABLE I
Swelling Characteristics of PEG-Crosslinked PMVE/MA Hydrogels, $N = 3$

Formulation (2 : 1) 15% PMVE/MA : PEG	% EWC	r_i[a]	$k_s.10^{-5}$[b]	S_{eq}%[c]
0% $NaHCO_3$	731 ± 15	71.67	14.05	714
1% $NaHCO_3$	860 ± 28	84.31	12.14	833
2% $NaHCO_3$	1109 ± 29	108.73	8.81	1111
5% $NaHCO_3$	7536 ± 210	738.82	7.39	10,000

[a] (g water/g gel)/min.
[b] (g gel/g water)/min.
[c] (g water/g gel).

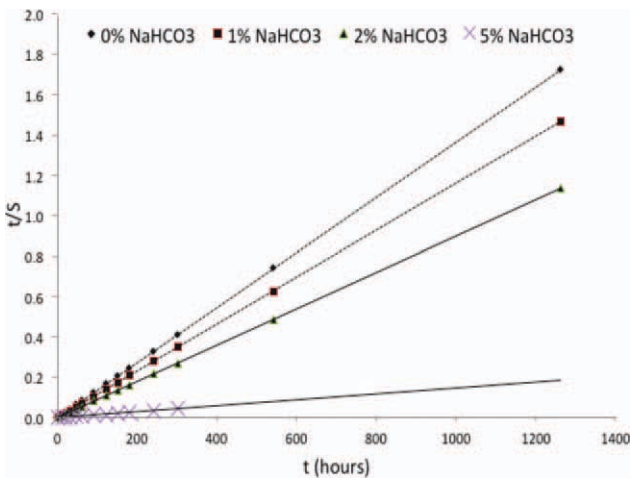

Figure 3 t/S versus t swelling curves of PEG-crosslinked PMVE/MA hydrogels containing different percentages of $NaHCO_3$. [Color figure can be viewed in the online issue, which is available at wileyonlinelibrary.com.]

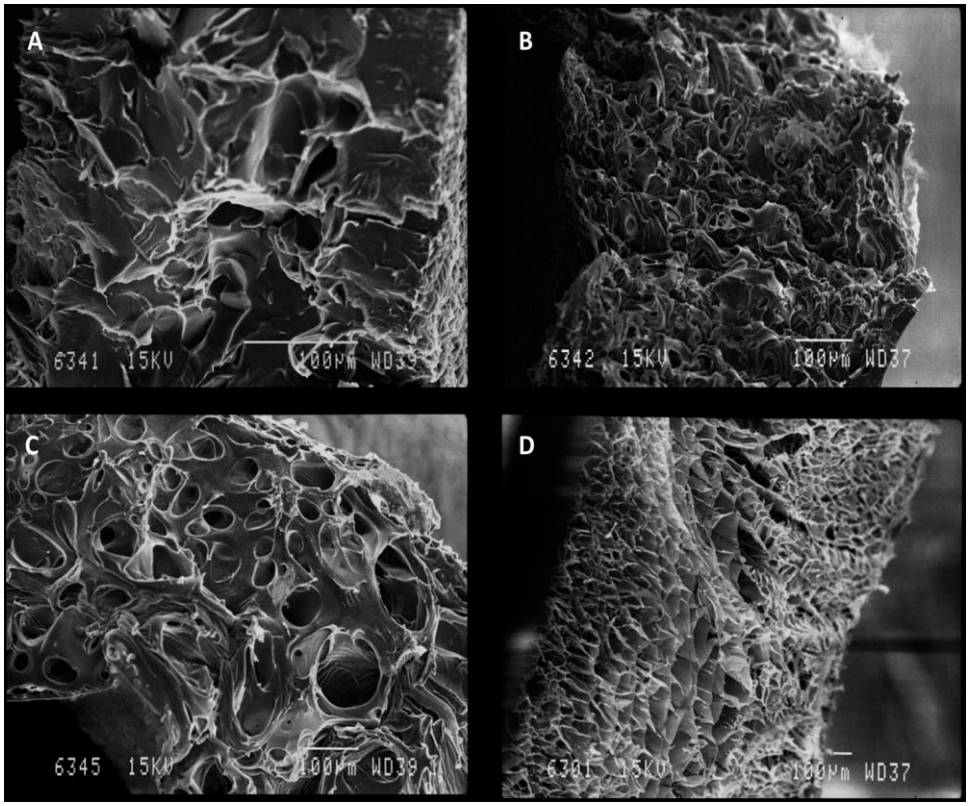

Figure 4 SEM micrographs hydrogels prepared from aqueous blends of 15% w/w PMVE/MA and 7.5% w/w PEG 10,000 containing (A) 0%, (B) 1%, (C) 2%, and (D) 5% w/w of $NaHCO_3$.

RESULTS AND DISCUSSION

Diffusion of solutes through hydrogels has a wide variety of applications in a variety of fields, but the interest in this study lies in the use of hydrogels as controlled drug delivery systems for macromolecules.[45] We have previously shown that PEG-crosslinked PMVE/MA hydrogels are held together by ester bonds and that permeation of solutes across equilibrium swollen hydrogels is dependent upon the solute's hydrodynamic radius.[32,33] However, permeation of a model macromolecule (insulin) through equilibrium swollen hydrogels was prevented due to its higher hydrodynamic radius. Therefore, in this study, porous hydrogels based on PEG-crosslinked PMVE/MA systems were prepared by a foaming technique (also called gas-blowing), where $NaHCO_3$ was selected as the pore-forming agent. Porous hydrogels were evaluated for their swelling and network parameters and *in vitro* permeation of insulin was studied. MN arrays were fabricated from these hydrogels and its application as a novel transdermal drug delivery device was evaluated.

The foaming process involves bubble generation, in which the polymer chains are crosslinked around gas bubbles generated by a "blowing agent."[46] Bubble size can be controlled either by the foaming agent (nature and concentration) or by the stirring conditions.[47] Foaming, or pore-forming, agents can be classified as: (a) physical foaming agents that expand when pressure is released (e.g., nitrogen and carbon dioxide) and (b) chemical foaming agents that decompose or react to form a gas (e.g., $NaHCO_3$ in the presence of acid). Inorganic carbonates such as, $CaCO_3$,[48] Na_2CO_3,[29,30] and $NaHCO_3$[29–31,49] have been extensively used as foaming agents. The major advantages of these pore-formers are that they are safe, cheap, and easy to use. Therefore, in this study, we have used $NaHCO_3$ as a pore-forming agent.

Figure 2 shows the swelling of hydrogels prepared from aqueous blends containing different concentrations of $NaHCO_3$. In general, increase in the $NaHCO_3$ concentration increased the swelling of the hydrogels. Addition of $NaHCO_3$ also affected the time to reach equilibrium-swollen state. For example, hydrogels prepared from aqueous blends containing 0% w/w of $NaHCO_3$ showed a significant ($P = 0.001$ in each case) increase in percentage swelling up until 5 h, after which increases in percentage swelling were not significant. In contrast, hydrogels prepared from aqueous blends containing 1% w/w $NaHCO_3$ showed a significant ($P = 0.008$) increase in percentage swelling up until 4.0 h, after which increases in percentage swelling were not significant. However, in the case of hydrogels prepared from aqueous blends containing

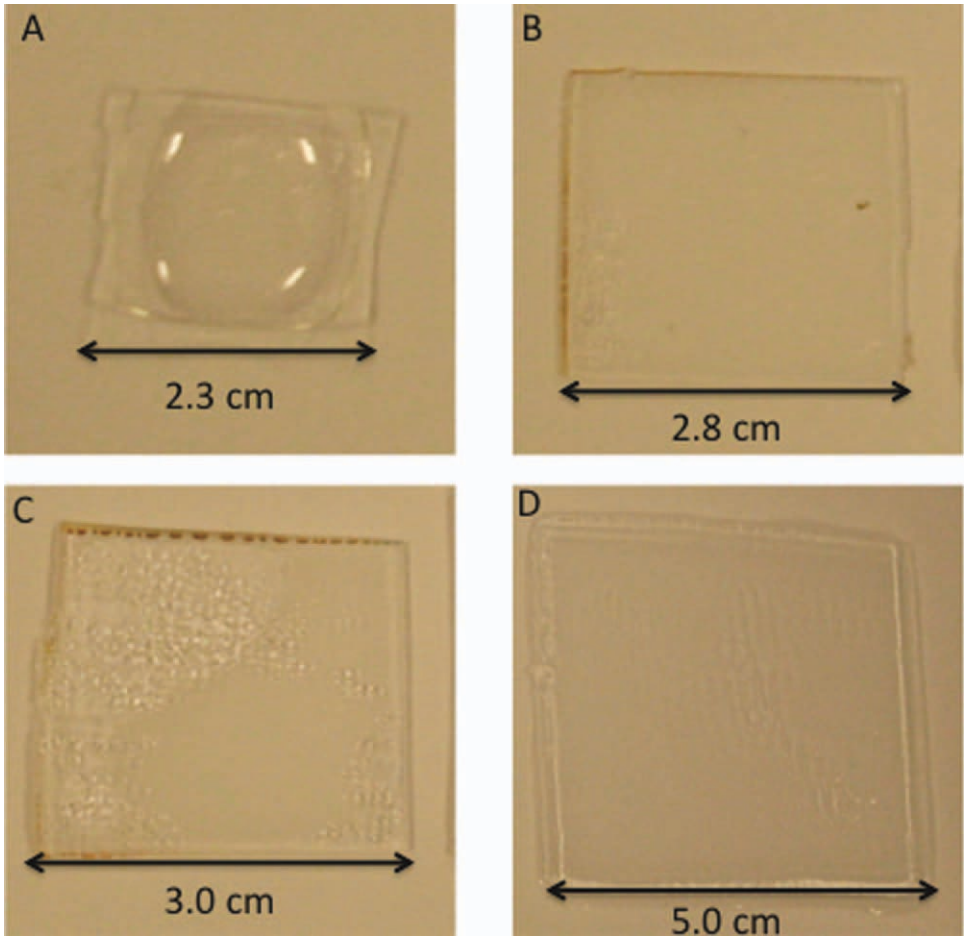

Figure 5 Digital photographs of equilibrium swollen hydrogels (with initial dimensions of 1 × 1 cm^2) prepared from aqueous blends of 15% w/w PMVE/MA and 7.5% w/w PEG 10,000 containing (A) 0%, (B) 1%, (C) 2%, and (D) 5% w/w of $NaHCO_3$ showing changes in respective dimensions. [Color figure can be viewed in the online issue, which is available at wileyonlinelibrary.com.]

5% w/w $NaHCO_3$, weight measurement was not possible after 6.0 h. This was due to very high swelling, which resulted in mechanically weak hydrogels.

The % EWC values shown in Table I were calculated from swelling studies using eq. (2). The % EWC values ranged from 731% ± 15% to 7536% ± 210% for hydrogels prepared from aqueous blends containing 0, 1, 2, and 5% w/w of $NaHCO_3$. Figure 3 shows the linear regression plots derived from swelling curves using eq. (3) and the respective swelling parameters are shown in Table I. Table I also shows initial rate of swelling (r_i) values of hydrogels, which increased with increase in the $NaHCO_3$ concentration. It was observed (Fig. 2) that hydrogels with higher $NaHCO_3$ contents showed greater initial swelling and reached equilibrium more quickly. The % EWC values of the hydrogels studied were significantly affected by the concentration of $NaHCO_3$. As can be seen from Table I, the theoretical equilibrium swellings of the hydrogels were comparable to their corresponding % EWC values.

TABLE II
Swelling Mechanisms and Diffusion Coefficients of Hydrogels Containing Different Percentages of $NaHCO_3$

15% w/w PMVE/MA : 7.5% w/w PEG (2 : 1)	n	Mechanism	Diffusion coefficient (D_i) × 10^{-6}, cm^2/min^{-1}
0% w/w $NaHCO_3$	0.85	Anomalous	2.46 ± 0.28
1% w/w $NaHCO_3$	0.92	Anomalous	2.29 ± 0.44
2% w/w $NaHCO_3$	0.60	Anomalous	2.07 ± 0.47
5% w/w $NaHCO_3$	0.86	Anomalous	3.93 ± 0.39

TABLE III
Network Parameters of PMVE/MA Crosslinked PEG Hydrogels Containing Different Percentages of $NaHCO_3$

15% w/w PMVE/MA: 7.5% w/w PEG (2 : 1)	$\Phi \times 10^{-2}$	χ	$M_c \times 10^5$ (g/mol)
0% w/w $NaHCO_3$	8.51	0.53	8.26
1% w/w $NaHCO_3$	6.22	0.52	31.64
2% w/w $NaHCO_3$	5.97	0.53	30.04
5% w/w $NaHCO_3$	0.91	0.50	3010.00

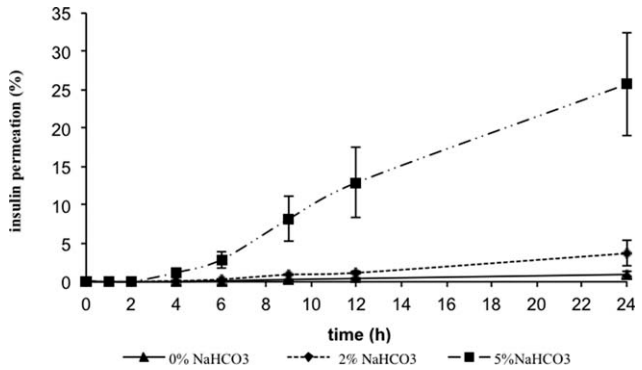

Figure 6 Cumulative amount of insulin permeated across equilibrium swollen hydrogels containing different loadings of $NaHCO_3$ (means ± SD, $n > 3$).

The SEM images of the equilibrium swollen hydrogels [Fig. 4(A–D)] show that $NaHCO_3$ incorporation affected the nature of these hydrogels. The observed porosity increased with an increase in the content of $NaHCO_3$, in comparison to hydrogels prepared without $NaHCO_3$. Digital photographs of these hydrogels are shown in Figure 5. Initially, all these hydrogels were 1×1 cm^2. This changed to 2.3, 2.8, 3.0, and 5.0 cm^2 for hydrogels containing 0, 1, 2, and 5% w/w of $NaHCO_3$, respectively. The swelling phenomenon of these hydrogels was directly related to the concentration of $NaHCO_3$. Cross-sectional SEM images showed that increase in $NaHCO_3$ content increased the pore-size of the equilibrium swollen and freeze-dried hydrogel membranes (Fig. 4). As a result, hydrogels prepared from aqueous blends containing 5% w/w of $NaHCO_3$ showed higher % EWC and higher initial swelling rates (r_i), followed by hydrogels prepared from aqueous blends containing 2%, 1%, and 0% w/w of $NaHCO_3$. In this study, the addition of $NaHCO_3$ as porosity generator into the formulation markedly affected the microstructure of the hydrogels. This is likely to be due to the release of CO_2 from $NaHCO_3$ during the swelling process leading to pore-formation in the hydrogels. Moreover, it is possible that $NaHCO_3$ further increases the void volume fraction and, therefore, reduces the dry hydrogel density.

TABLE IV
Amount of Insulin Permeated Across PMVE/MA-PEG Membranes Containing 0, 2, and 5% w/w $NaHCO_3$ at 24 h (Means ± SD, $n > 3$)

	Amount of insulin permeated at 24 h	
$NaHCO_3$ loading (%)	μg	%
0	1.88 ± 0.64	0.94 ± 0.32
2	7.36 ± 3.22	3.68 ± 1.61
5	51.41 ± 13.36	25.71 ± 6.68

Since the density is related to the porosity of the hydrogels, the higher the porosity the lower the density. Consequently, the equilibrium swelling capacities of the porous hydrogels are also much higher than those of the conventional hydrogels.[41]

The diffusional exponent, n, was found be greater than 0.5 for all hydrogels (Table II), as calculated from eq. (4), indicating an anomalous (non-Fickian) type diffusion. During anomalous diffusion, the relative rate of solvent diffusion (R_{diff}) is approximately equals to relative rate of chain relaxation (R_{relax}) i.e., $R_{diff} - R_{relax}$.[49] In addition, the diffusion coefficient determined from eq. (5), is also shown in Table II. The initial diffusion coefficients (D_i), were between 2.07×10^{-6} to 3.93×10^{-6} cm^2/min for hydrogels prepared from aqueous blends of 15% w/w of PMVE/MA containing 0 to 5% w/w $NaHCO_3$. Initial diffusion values of 5% w/w $NaHCO_3$ was significantly ($P > 0.05$ in each case) higher than 0, 1, and 2% w/w $NaHCO_3$ hydrogels. The lower initial diffusion values of the hydrogels containing 0, 1, and 2% w/w $NaHCO_3$ was due to its lower swelling percentage than compared to hydrogels containing 5% w/w $NaHCO_3$, as shown in Figure 2.

The polymer volume fraction (ϕ), determined using eq. (7), ranged from 0.91 to 8.51×10^{-2} for hydrogels containing 0 to 5% w/w of $NaHCO_3$ (as shown in Table III). The M_c determined by the equilibrium swelling method using eq. (6), is also shown in Table III. The values of M_c were observed to range from 8.26 to 3010.00×10^{-2} 10^5 g/mol for hydrogels prepared from aqueous blends of 15% w/w of PMVE/MA containing 0 to 5% $NaHCO_3$, respectively. In addition, the hydrogels showed almost similar polymer–water interaction parameter (χ) values. As described earlier, the change in the ϕ value of the hydrogels represented a similar trend, where the ϕ decreased with increase in the $NaHCO_3$ content. On the other hand, $NaHCO_3$ content had no significant effect on

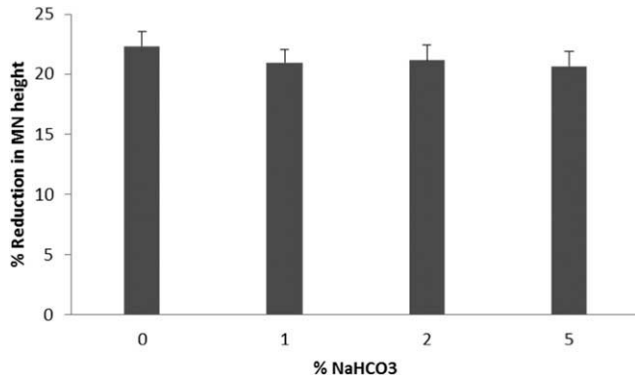

Figure 7 Percentage reduction in height of MN arrays prepared from PMVE/MA-PEG formulations containing varying amounts of $NaHCO_3$, following application of a compression force of 0.36 N per needle. Mean + SD, $n = 9$.

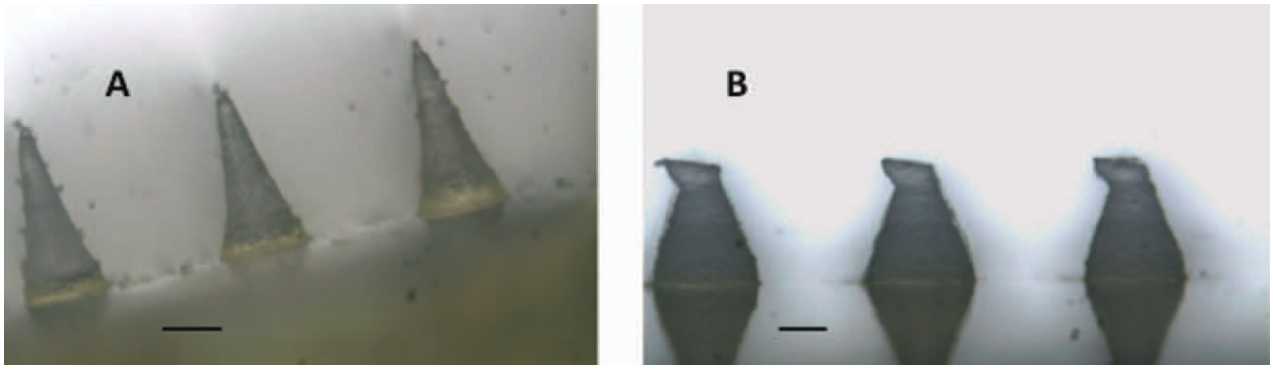

Figure 8 Representative light microscopy images of MN arrays (containing 5% $NaHCO_3$) before (A) and after (B) application of a compression force of 0.36 N per MN. Scale bar represents 200 μm. [Color figure can be viewed in the online issue, which is available at wileyonlinelibrary.com.]

the χ parameter of the crosslinked hydrogels. The network parameters clearly indicate that, with increase in $NaHCO_3$ content, the number of crosslinks per unit volume also increased causing an increase in the molecular weight between two crosslinks (M_c).

Figure 6 shows the cumulative permeation of insulin across equilibrium swollen PEG-crosslinked PMVE/MA hydrogel membranes. The results indicated that the percentage permeation of insulin increased with increasing content of $NaHCO_3$ in hydrogel membranes. For example, the percentage cumulative permeation of insulin after 24 h was ~ 0.9%, 3.7%, and 25.7% across hydrogels containing 0, 2, and 5% w/w $NaHCO_3$, respectively. The mean amount of insulin permeated was ~ 1.9 μg, 7.4 μg, and 51.4 μg after 24 h, respectively (Table IV). Statistical analysis revealed that the cumulative amount of insulin permeated across hydrogel membranes containing 0% $NaHCO_3$ differed significantly from the amount permeated across hydrogel membranes containing 2 and 5% w/w $NaHCO_3$ ($P = 0.034$ and $P = 0.021$, respectively). In addition, the amount of insulin permeated across hydrogel membranes containing 2% w/w $NaHCO_3$ was statistically different from the amount permeated across hydrogel membranes containing 5% w/w $NaHCO_3$ ($P = 0.034$). These findings may be attributed to high % EWC and M_c, of hydrogels containing pore-forming agents. Therefore, addition of the pore-forming agent resulted in increase in the pore-size of the hydrogels (as seen from SEM images) and resulted in decrease of their crosslink density, which resulted in higher permeation of insulin. In contrast, the lower permeation of insulin through the hydrogels without pore-forming agent could be attributed to its high hydrodynamic radius.

The Stokes–Einstein Equation, in an ideal aqueous medium, predicts that permeability declines as a linear function of molecular radius.[50] Furthermore, the rate of solute diffusion is determined by the probability of a void space in the hydrogel.[50,51] Increasing the size of the void space may, therefore, promote the diffusion of a solute of high hydrodynamic radius, such as the model peptide insulin in the present study. As a result, to allow the diffusion of insulin across swollen hydrogels, investigated in this

TABLE V
Determination of the Force Required for MN Insertion into Excised Neonatal Porcine Skin (Mean ± SD, $n = 5$)

	% of holes created		
	Force (N per needle)		
% $NaHCO_3$	0.01	0.02	0.03
0	0 ± 0	0 ± 0	100 ± 0
1	0 ± 0	0 ± 0	100 ± 0
2	0 ± 0	0 ± 0	100 ± 0
5	0 ± 0	0 ± 0	100 ± 0

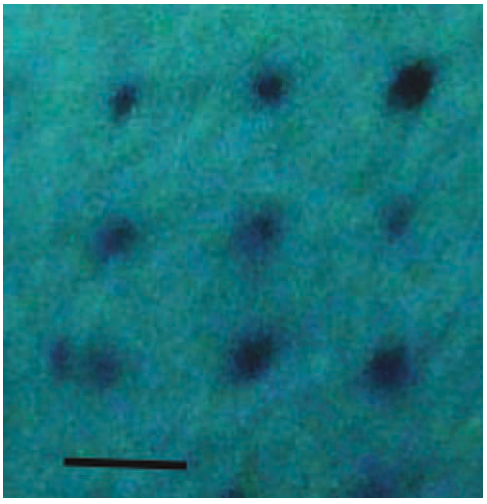

Figure 9 Representative digital image of the methylene blue stained pores created within the skin following application of a MN array to excised neonatal porcine skin at a force of 0.03 N per needle. Scale bar represents a length of 300 μm. [Color figure can be viewed in the online issue, which is available at wileyonlinelibrary.com.]

Figure 10 Representative OCT image showing the depth of MN penetration following MN (5% $NaHCO_3$) application to neonatal porcine skin. Scale bar represents a length of 300 μm. [Color figure can be viewed in the online issue, which is available at wileyonlinelibrary.com.]

study, it was necessary to add agents, which increase the pore-size and, therefore, void space, of the hydrogels.

Figure 7 shows the results of the mechanical strength testing of MN arrays prepared from PEG-crosslinked PMVE/MA formulations containing varying amounts of $NaHCO_3$. It was found that the addition of $NaHCO_3$ had no effect upon the percentage reduction of MN height following the application of a compression force of 0.36 N per needle ($P > 0.05$ in all cases). For example, the percentage reduction in MN height was found to be 22.31 ± 1.21, 20.95 ± 1.05, 21.14 ± 1.27, and 20.63 ± 1.21% for hydrogel formulations containing 0, 1, 2, and 5% $NaHCO_3$, respectively. Figure 8 shows representative images of MN arrays (containing 5% $NaHCO_3$) before and after application of a compression force of 0.36 N per needle. It was found that all MN formulations prepared were capable of penetrating the skin once the force of application was = 0.03 N per needle (Table V). Figure 9 shows a representative digital image highlighting the creation of methylene blue stained pores following application of a MN array (containing 5% $NaHCO_3$) to excised neonatal porcine skin at a force of 0.03 N per needle.

TABLE VI
OCT Assessment of MN Penetration into Neonatal Porcine Skin Following Application Using a Spring Activated Applicator at a Force of 11.0 N Per Array (Mean ± SD, $n = 25$)

% $NaHCO_3$	MN penetration depth (μm)	Pore width (μm)	Base plate/SC distance (μm)
0	463.32 ± 4.95	214.07 ± 8.85	146.48 ± 4.27
5	461.61 ± 7.13	214.62 ± 5.71	146.57 ± 6.35

OCT analysis revealed that, following insertion into neonatal porcine skin at a force of 11.0 N per array, the entirety of the MN length did not enter the skin. A clear gap of ~ 146 μm was evident between the surface of the skin and the MN base plate (Fig. 10). Furthermore, it was found that there

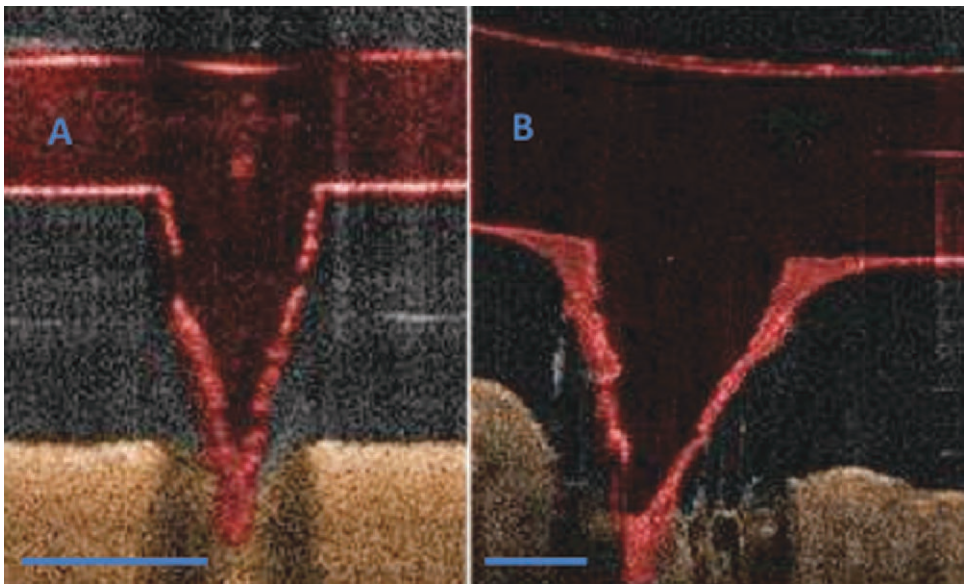

Figure 11 Representative OCT images of hydrogel forming MN array (containing 5% $NaHCO_3$) before (A) and after (B) insertion into neonatal porcine skin for a period of 24 h. Scale bar represents a length of 300 μm. [Color figure can be viewed in the online issue, which is available at wileyonlinelibrary.com.]

TABLE VII
OCT Assessment of Changes in MN Dimensions Following Residence Within Neonatal Porcine Skin for a Period of 24 h (Mean ± SD, $n = 25$)

0% $NaHCO_3$			5% $NaHCO_3$		
Time (h)	MN height (μm)	MN width (μm)	Time (h)	MN height (μm)	MN width (μm)
0	609.80 ± 6.57	303.76 ± 6.65	0	604.23 ± 9.15	306.23 ± 6.46
24	737.38 ± 11.74	551.96 ± 9.63	24	825.81 ± 10.14	622.46 ± 8.98

was no difference in the penetration of MN based upon PEG-crosslinked PMVE/MA formulations prepared from aqueous blends containing either 0 or 5% $NaHCO_3$, with the depths of penetration achieved being 463.32 ± 4.95 and 461.61 ± 7.13 μm (Table VI), respectively ($P = 0.893$). For the first time, OCT was used within this study to identify the in-skin changes in MN dimensions that occur following insertion of these hydrogel forming MN arrays into neonatal porcine skin. As can be seen from Figure 11, once inserted into skin, these MN arrays are capable of absorbing skin interstitial fluid to form a swollen hydrogel matrix. This is evident by an increase in the MN height and MN width of each MN on an array following insertion into the skin for a period of 24.0 h (Table VII). It was also noted that the addition of 5% $NaHCO_3$ resulted in an increase the MN height ($P = 0.018$) and MN width ($P = 0.012$) observed, in comparison to a MN array based on PEG-crosslinked PMVE/MA containing 0% $NaHCO_3$.

Table VIII presents results from insulin content analysis by HPLC. Investigation of insulin recovery from the patches revealed that ~ 30% of insulin was lost during the manufacturing process. As can be appreciated from Table V, the mean percentage recovery of insulin from the patches loaded at 5.0 mg/cm^2 was ~ 69.9% after 48 h drying at room temperature (0 days). Statistical analysis revealed that the amount of insulin recovered was significantly different from the theoretical value of 5 mg/cm^2 ($P = 0.003$), which could be an indication of potential interaction between insulin and the components of the patch. Storage of insulin loaded patches at 4.0°C over 28 days did not have any further negative influence on insulin content. Statistical analysis showed that there was no significant difference between the amount of insulin adhesive patches after 28 days of storage at 4.0°C in comparison to the insulin amount recovered at day 0 ($P = 0.059$). To assess structural integrity of insulin incorporated into PMVE/MA-TPM patches CD spectra were obtained. Figure 12 presents generated results. As can be appreciated, incorporation of insulin into PMVE/MA-TPM patches resulted in the decrease of the intensity of two negative bands at 208 and 222 nm, which is indicative of the reduction in alpha-helix content.[52–55] Thus, the secondary structure of insulin was altered by incorporation into patches.

TABLE VIII
Determination of Insulin Content in Adhesive Patches at Different Time Points by HPLC (Means ± SD, $n = 4$)

Theoretical insulin loading (mg/cm^2)		Recovery	
		0 day	28 days
5.00	mg	3.63 ± 0.31	3.36 ± 0.06
	%	69.89 ± 5.95	67.16 ± 1.26

Figure 13 presents the cumulative amount of insulin permeated across dermatomed neonatal porcine skin after release from adhesive patches, loaded with 5 mg/cm^2 insulin, and integrated with MNs prepared from aqueous blends of 15% w/w PMVE/MA and 7.5% w/w PEG 10,000 containing 0 and 5% w/w $NaHCO_3$. The results revealed that the use of PEG-crosslinked PMVE/MA hydrogel MNs containing 5% w/w $NaHCO_3$ led to an increase in the cumulative amount of insulin released from adhesive patches and permeated across porcine neonatal skin in comparison to the amount of insulin delivered when hydrogel MNs without $NaHCO_3$ were used. The mean percentage permeation of insulin from adhesive patches integrated with 0 and 5% w/w $NaHCO_3$-PMVE/MA-PEG MNs across porcine skin was found to be ~ 20.6% and 52.5% after 24.0 h,

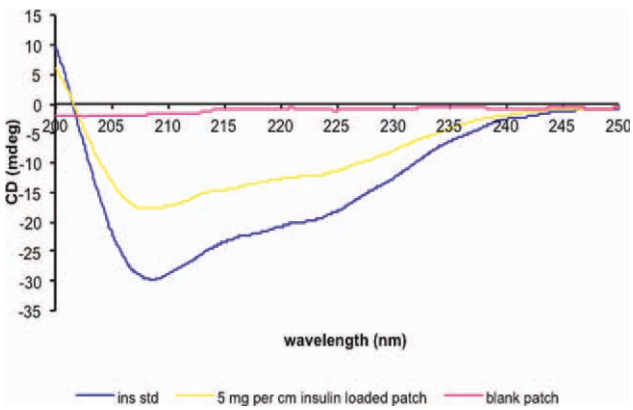

Figure 12 CD spectra of insulin encapsulated and released from PMVE/MA-TPM patches (yellow) and blank PMVE/MA-TPM patch without insulin (pink) and CD spectrum of insulin standard solution (dark blue). [Color figure can be viewed in the online issue, which is available at wileyonlinelibrary.com.]

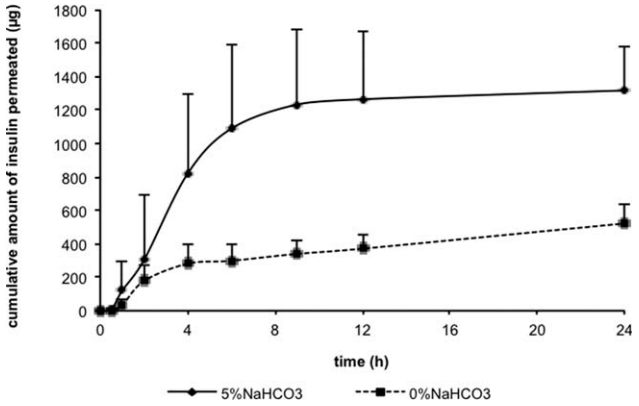

Figure 13 Cumulative amount of insulin permeated across neonatal porcine skin from adhesive patches integrated with hydrogel MNs prepared from aqueous blends of 15% w/w PMVE/MA and 7.5% w/w PEG 10,000 containing 0 and 5% w/w of $NaHCO_3$ (means ± SD, $n = 4$). [Color figure can be viewed in the online issue, which is available at wileyonlinelibrary.com.]

respectively (Table IX). Statistical analysis revealed that there was a significant difference between the insulin amount released from the patches integrated with 0%-$NaHCO_3$-PMVE/MA-PEG-based MNs (522.2 µg) and 5%-$NaHCO_3$-PMVE/MA-PEG-based MNs (1317.8 µg) ($P = 0.021$). No detectable amounts of insulin permeated across dermatomed neonatal skin after 24 h when adhesive patches not integrated with PMVE/MA-PEG-based MN were applied to the skin. Importantly, as can be seen in Figure 14, all MN in each array were removed intact from skin after 24 h, indicating that MN arrays based upon the tested formulations have sufficient mechanical strength to resist compression and/or breakage following insertion into skin for periods up to 24 h.

CONCLUSION

The results of this study suggest that hydrogels containing a pore-forming agent could be effectively applied in controlled release devices for high molecular weight compounds, such as peptides and proteins.

TABLE IX
Amount of Insulin Released from PMVE/MA-TPM Patches, Loaded with Theoretical Insulin Loadings of 5 mg/cm^2, Integrated with Hydrogel MNs Prepared from Aqueous Blends of 15% w/w PMVE/MA and 7.5% w/w PEG 10,000 Containing 0% and 5% w/w $NaHCO_3$ Across Dermatomed Neonatal Porcine Skin After 24 h (means ± SD, $n = 4$)

PMVE/MA-PEG MN formulation [% (w/w) of $NaHCO_3$]	Amount of insulin released at 24 h	
	µg	%
0	522.15 ± 109.06	20.62 ± 4.31
5	1317.82 ± 267.18	52.48 ± 9.01

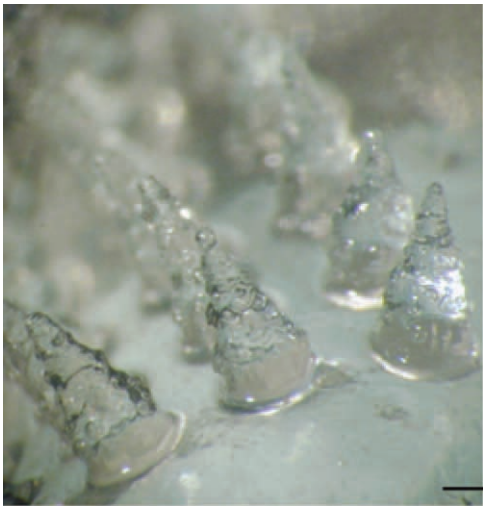

Figure 14 Representative light microscopy image showing an intact hydrogel MN array (containing 5% $NaHCO_3$) following removal from neonatal porcine skin after a period of 24 h. Scale bar represents a length of 300 µm. [Color figure can be viewed in the online issue, which is available at wileyonlinelibrary.com.]

Of significant importance, we have shown here, for the first time, that these hydrogels can be processed to make MN arrays that are mechanically strong enough, in the dry state, to penetrate the *stratum corneum* of skin. Such systems then swell in skin interstitial fluid to produce continuous, unblockable, conduits allowing transdermal macromolecular drug delivery from an attached patch-type drug reservoir. Surprisingly, all MN in each array were removed from skin intact after 24 h, indicating retention of mechanical strength, a phenomenon unusual in hydrogels. These delivery devices have major potential, since they have the potential to overcome many of the current problems associated with MN-mediated delivery, such as limited drug doses, two step applications and deposition of polymer in skin.[55] We are now extensively investigating these integrated hydrogel MN-patch designs for a range of applications in transdermal delivery of macromolecules.

References

1. Mehrdad, H.; Amir, A.; Pedram, R. Adv Drug Deliv Rev 2008, 60, 1638.
2. Hennink, W. E.; vanNostrum, C. F. Adv Drug Deliv Rev 2002, 54, 13.
3. Mark, E. B.; Vishal, S. Int J Pharm 2008, 364, 188.
4. Sunil, K. B.; Surinderpal, S. React Funct Polym 2006, 66, 431.
5. Wang, J.; Wu, W. Eur Polym J 2005, 41, 1143.
6. Allan, S. H. Adv Drug Deliv Rev 2002, 54, 3.
7. Stoy, V. A. In Encyclopaedia of Pharmaceutical Technology; Swarbrick, J., Boylan, J.C., Eds.; Marcel Dekker: New York, 1999; p 91.
8. Lowmann, A. M.; Peppas, N. A. In Encyclopaedia of Controlled Drug Delivery; Mathiowitz, E., Ed.; John Wiley & Sons: New York, 1999; p 397.

9. Kashyap, N.; Kumar, N.; Kumar, M. N. Crit Rev Ther Drug Carrier Syst 2005, 22, 107.
10. Robert, L.; Peppas, N. A. AIChE J 2003, 49, 2990.
11. Gehrke, S. H. In Transport Process in Pharmaceutical Systems; Amidon, G. L., Lee, P. I., Topp, E. M., Eds.; Marcel Dekker: New York, 2000; p 473.
12. Gehrke, S. H.; Lee.P. I. In Specialized Drug Delivery Systems; Tyle, P., Ed.; Marcel Dekker: New York, 1990; p 333.
13. Veiga, F.; Salsa, M. T.; Pina, E. Drug Dev Ind Pharm 1998, 24, 1.
14. Kim, B.; Kristen, L. F.; Peppas, N. A. J Appl Polym Sci 2003, 89, 1606.
15. Moussaoui, M.; Benylas, M.; Wahl, P. J Chromatogr 1991, 558, 71.
16. Peppas, N. A., Ed. In Hydrogels in Medicine and Pharmacy. CRC Press: Boca Raton, FL; Vol.1, p 28. (Biochim Biophys Acta 1987, 1304, 179).
17. Knack, I.; Beckert, W. U. S. Pat. 5,002, 814, 1991.
18. Amsden, B. Macromolecules 1998, 31, 8382.
19. Chung, T. W.; Yang, J.; Akaike, T.; Cho, K. Y.; Nah, J. W.; Kim, S. I.; Cho, C. S. Biomaterials 2002, 23, 2827.
20. Kang, H. W.; Tabata, Y.; Ikada, Y. Biomaterials 1999, 20, 1339.
21. Noble, L.; Gray, A. I.; Sadiq, L.; Uchegbu, I. F. Int J Pharm 1999, 192, 173.
22. Von, H. D.; Zachariah, S.; Heschel, I.; Kuhling, H.; Schoof, H.; Hafemann, B.; Pallua, N. Biomaterials 2001, 22, 429.
23. Yoon, J. J.; Park, T. G. J Biomed Mater Res 2001, 55, 401.
24. Zhang, R.; Ma, P. X. J Biomed Mater Res 1999, 45, 285.
25. Mikos, A. G.; Bao, Y.; Cima, L. G.; Ingber, D. E.; Vacanti, J. P.; Langer, R. J Biomed Mater Res 1993, 27, 183.
26. Krauch, C. H.; Sanner, A. Nat Wissenscheften 1968, 55, 539.
27. Oxley, H. R.; Corkhill, P. H.; Fitton, J. H.; Tighe, B. J. Biomaterials 1993, 14, 1065.
28. Lam, C. X. F.; Mo, X. M.; Teoh, S. H.; Hutmacher, D. W. Mater Sci Eng 2002, 20, 49.
29. Park, H.; Park, K. Hydrogel foams: A new type of fast swelling hydrogels. In The 20th Annual Meeting of the Society for Biomaterials, Boston, Abstract #158, 1994.
30. Park, H.; Park, K. Proc Int Symp Control Rel Bioact Mater 1994, 21, 21.
31. Chen, H.; Zhu, H.; Zheng, J.; Mou, D.; Wan, J.; Zhang, J.; Shi, T.; Zhao, Y.; Xu, H.; Yang, X. J Control Release 2009, 139, 63.
32. Singh, T. R. R.; McCarron, P. A.; Woolfson, A. D.; Donnelly, R. F. Eur Polym J 2009, 45, 1239.
33. Singh, T. R. R.; Woolfson, A. D.; Donnelly, R. F. J Pharm Pharmacol 2010, 62, 1.
34. Hydrodynamic Reference. Available at: http://www.malvern.com/labeng/industry/protein/protein_solutions.htm. Accessed on 15th November 2010.
35. McCarron, P. A.; Woolfson, A. D.; Donnelly, R. F.; Andrews, G. P.; Zawislak, A.; Price, J. H. J Appl Polym Sci 2004, 91, 1576.
36. Wang, J.; Wu, W. Eur Polym J 2005, 41, 1143.
37. Peniche, C.; Cohen, M. E.; Vazquez, B.; Roman, J. S. Polymer 1997, 38, 5977.
38. Bajpai, A. K.; Bajpai, J.; Sandeep, S. React Funct Polym 2001, 50, 9.38.
39. Paul, J. F.; John, R. J. J Chem Phys 1943, 11, 512.
40. Tuncer, C.; Simin, K.; Gokhan, D. J Appl Polym Sci 2006, 101, 1756.
41. Migalska, K.; Morrow, D. I.; Garland, M. J.; Singh, T. R. R.; Woolfson, A. D.; Donnelly, R. F. Pharm Res 2011, 28, 1919.
42. Donnelly, R. F.; Majithiya, R.; Singh, T. R. R.; Morrow, D. I.; Garland, M.; Demir, Y. K.; Migalska, K.; Ryan, E.; Gillen, D.; Scott, C. J.; Woolfson, A. D. Pharm Res 2011, 28, 41.
43. Donnelly, R. F.; Garland, M. J.; Morrow, D. I.; Migalska, K.; Singh, T. R. R.; Majithiya, R.; Woolfson, A. D. J Control Release 2010, 147, 333.
44. Masaro, L.; Zhu, X. X. Prog Polym Sci 1999, 24, 731.
45. Park, J. S.; Park, J. W.; Ruckenstein, E. J Appl Polym Sci 2001, 82, 1816.
46. Chevalier, E.; Dominique, C.; Christelle, P.; Marylene, V. J Pharm Sci 2008, 97, 1135.
47. Mahdavinia, G. R.; Mousavi, S. B.; Karimi, F.; Marandi, G. B.; Garabaghi, H.; Shahabv, S. Polym Lett 2009, 3, 279.
48. Del, R. R. P.; Wolke, J. G. C.; Vallet-Regi, M.; Jansen, J. A. Biomaterials 2002, 23, 3673.
49. Ritger, P. L.; Peppas, N. A. J Control Release 1987, 5, 37.
50. Brian, A. Macromolecules 1998, 31, 8382.
51. Estey, T.; Kang, J.; Schwendeman, P.; Carpenter, J. J Pharm Sci 2006, 95, 1626.
52. Henricus, M.; Johnon, K.; Banerje, I. Bioconjugate Chem 2008, 19, 2394.
53. Wang, J.; Wu, J.; Zhang, Z.; Zhang, D.; Wang, L.; Xu, L.; Guo, B.; Li, H.; Tong, J. Chin Chem Lett 2005, 16, 1105.
54. Wangoo, N.; Suri, C.; Shekawat, G. App Phys Lett 2008, 92, ID 133104.
55. Garland, M. J.; Migalska, K.; Mahmood, T. M. T.; Singh T. R. R.; Woolfson, A. D.; Donnelly, R. F. Expert Opin Med Dev 2011, 8, 455.